Quest for a Rational Molecular Design of Alkyl–Distyrylbenzene Liquid by Substitution Pattern Modulation

Xiao Zheng,[a,b] Kazuhiko Nagura,[b] Tomohisa Takaya,[c] Kenjiro Hashi,[d] and Takashi Nakanishi*[a,b]

[a] X. Zheng, Prof. Dr. T. Nakanishi
Division of Soft Matter, Graduate School of Life Science
Hokkaido University, Kita 10, Nishi 8, Kita-ku, Sapporo 060-0810, Japan
[b] X. Zheng, Dr. K. Nagura, Prof. Dr. T. Nakanishi
International Center for Materials Nanoarchitectonics (WPI-MANA)
National Institute for Materials Science (NIMS), 1-1 Namiki, Tsukuba 305-0044, Japan
Email: nakanishi.takashi@nims.go.jp
[c] Prof. T. Takaya
Department of Electrical and Electronic Engineering, Faculty of Engineering
Toyama Prefectural University, 5180 Kurokawa, Imizu, Toyama 939-0398, Japan
[d] Dr. K. Hashi
Research Center for Advanced Measurement and Characterization
National Institute for Materials Science (NIMS), 3-13 Sakura, Tsukuba 305-0003, Japan

Abstract:

Alkyl-π functional molecular liquids (FMLs) are of interest for fabricating soft electronic devices due to their fluidic nature and innate optoelectronic functions from the π-conjugated moiety. However, predictable development of alkyl-π FMLs with the desired liquid and optoelectronic properties is challenging. A series of alkyl–distyrylbenzene (DSB) liquids was studied in terms of the substituent position effect by attaching 2-octyldodecyl chains at (2,4-), (2,5-), (2,6-), and (3,5-). The effect of the alkyl chain length was investigated by attaching 2-hexyldecyl, 2-decyltetradecyl ($C_{10}C_{14}$), and 2-dodecylhexadecyl at the (2,5-) substituent position. The 2,5-$C_{10}C_{14}$ substituent pattern constructed a superior alkyl–DSB liquid with a lower viscosity, intrinsic optical properties, and high thermal- and photo-stabilities. The discovered 2,5-$C_{10}C_{14}$ was applied to dicyanostyrylbenzene and comparable liquid physical and optical superiorities were confirmed. This molecular design is useful for creating alkyl-π FMLs with the aforementioned advantages, which are applicable for deformable and flowable optoelectronic devices.

Introduction

Stretchable, foldable, and free-shapeable optoelectronic devices such as wearable/implantable energy harvesters, sensors, and actuator robotics applicable in healthcare and cyberspace technologies have become high-priority research targets in recent years.[1] There is a need for optoelectronically active materials to be fabricated into these highly flexible devices. One of the promising functional soft materials for the above-mentioned targets is alkyl-π functional molecular liquids (FMLs), which are receiving considerable attention because they exhibit a fluidic nature and innate optoelectronic functions from the π-conjugated moiety.[2a] Bulky yet flexible and low-melting branched alkyl chains are attached on the periphery of rigid π-conjugated molecules by alkyl-π engineering, and the room temperature liquid state of the π-conjugated molecules can be produced.[2b] Diverse FMLs such as nanocarbon liquids,[3] luminescent liquids,[4] macrocyclic liquids,[5] and conjugated polymer fluids[6] have been developed in the past decade. Several alkyl-π FMLs have been explored as substances on flexible/stretchable devices, such as microfluidic organic light emitting diodes (OLEDs)[7] and vibration-powered electret generators.[5a, 6c]

Predictable development of an alkyl-π FML possessing the desired fluidity, optoelectronic properties, and high thermal- and photo-stabilities as a thermodynamically stable liquid at room temperature is a challenging task. In reality, several intractable issues were identified in previous investigations of alkyl-π FMLs. Generally, richer optoelectronic functions such as charge-storage electret ability,[5a] electrochromic properties,[8] and photoconductivity[9] were seen in relatively larger π-conjugated compounds, i.e., porphyrins,[5a] phthalocyanines,[5c-d] and fullerenes.[3] However, the liquid viscosity of 15.7–220×10^3 Pa·s, was much higher than that of alkyl-π liquids with a smaller π-conjugated moiety, i.e., tetrazine[10] and naphthalene[4d] with 28.0–85.3×10^{-3} Pa·s. Moreover, an unexpected crystallization from the metastable supercooled liquid (SCL) state of the alkyl-π FMLs was occasionally found under prolonged storage at room temperature or with external mechanical stimuli, which is not beneficial for their consistent performance in deformable and flowable applications.[11]

Substitution pattern modulation is a strategy adopted in this study toward the quest for a rational molecular design of alkyl-π FMLs possessing a lower viscosity, intrinsic optical properties from the π-conjugated unit, high thermal- and photo- stabilities, and good synthetic yield. In biology, even just one altered genetic sequence undergoes mutation.[12] Similarly, the characteristics of π-conjugated compounds, such as the conformational,[13a] thermal,[13b] photophysical,[13c] and electrochemical[13d] properties, can be tuned by different substitution patterns. Therefore, taking advantage of the substitution pattern modulation could regulate the alkyl-π FML functions at both the molecular level and in the bulk liquid state. A π-conjugated moiety that allows substitution in different numbers and positions should match our current target so a larger π-conjugated moiety is not considered. Therefore, a suitable molecular model is required to study the effect of the substitution pattern on alkyl-π FMLs.

Distyrylbenzene (DSB) is a well-known dye with superior blue luminescence and facile derivatization.[14] Since Kaufmann *et al.* first prepared DSB in 1917, the substitution pattern effect has been investigated to improve the solubility.[14a-b] To attenuate the luminescence quenching of DSB compounds, Protasiewicz *et al.* introduced bulky dimesityl groups at the (2,6-) position of both terminal phenyl units to prevent π–π interactions among the DSB moieties.[14c] The photophysical properties of the DSB compounds were well understood in different states, such as in a solution

of *J*- and *H*-aggregates. Notably, in 2012, our group utilized alkyl-π engineering to achieve solvent-free luminescent alkyl–DSB liquids at room temperature, which were used as a small dye dopant dispersion medium for a paintable white light luminescent composite.[4a] However, the substitution pattern effect on the alkyl–DSB liquids to clarify the liquid physical and optical properties as well as to improve the phase, thermal, and photostability has not yet been thoroughly investigated. We believe that DSB is an appropriate π-conjugated moiety in size and structure to systematize the substitution pattern by introducing branched alkyl chains.

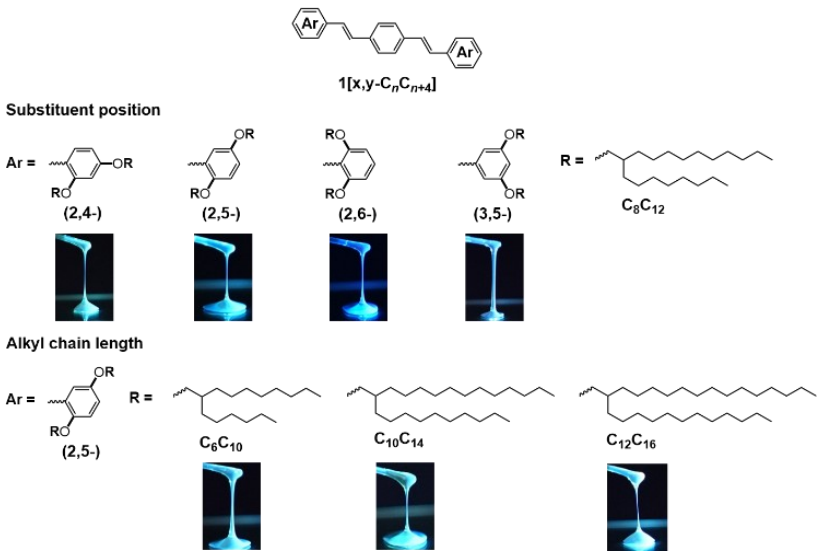

Figure 1. Chemical structure and photo images of **1[x,y-C$_n$C$_{n+4}$]** compounds. Photo images were taken in the solvent-free liquid state under UV 365 nm irradiation at room temperature. Notably, except for **1[2,6-C$_8$C$_{12}$]**, **1[2,5-C$_{10}$C$_{14}$]**, and **1[2,5-C$_{12}$C$_{16}$]**, the photo images taken of other compounds are in their SCL state.

Here, the focus is on two viewpoints. The first is the substituent position effect where 2-octyldodecyl (C_8C_{12}) chains are attached at different substituent positions, e.g. (2,4-), (2,5-), (2,6-), and (3,5-), through ether linkages on both terminal phenyl units so that these four compounds are regioisomers. The second viewpoint is the effect of the alkyl chain length, particularly 2-hexyldecyl (C_6C_{10}), 2-decyltetradecyl ($C_{10}C_{14}$), and 2-dodecylhexadecyl ($C_{12}C_{16}$) as well as the C_8C_{12} chains at the (2,5-) substituent position. These regioisomers and the alterations of the alkyl chain length on DSB are denoted as **1[x,y-C$_n$C$_{n+4}$]** (Figure 1). Rheology was used to measure the viscosity, and the influential factors on the viscosity were investigated by gel

permeation chromatography (GPC), solid-state nuclear magnetic resonance (SSNMR), and positron surface analysis (PSA). The thermal properties were mainly investigated by differential scanning calorimetry (DSC). Liquid-structure analysis as well as π–π interactions of the DSB units were evaluated with small- and wide-angle X-ray scattering (SWAXS) and optical investigations such as ultraviolet-visible (UV-Vis) absorption and fluorescence studies. With these thorough investigations on a series of **1[x,y-C$_n$C$_{n+4}$]** compounds, we specified the substitution pattern for constructing an alkyl–DSB liquid possessing a lower viscosity, inherent optical properties of the DSB core unit, and high thermal- and photo-stabilities as a thermodynamically stable liquid at room temperature.

Results and Discussion

2.1 Synthesis

Alkyl–DSB compounds, **1[x,y-C$_n$C$_{n+4}$]**, were synthesized according to previous literature including Appel, Williamson, and Horner–Wadsworth–Emmons reactions at the gram scale (Supplementary Information (SI), Schemes S1–S3).[3c,4a] The final target compounds were purified by silica-gel column chromatography and preparative GPC. The identification of these compounds was unambiguously carried out by ^{1}H and ^{13}C nuclear magnetic resonance (NMR) spectroscopy and matrix-assisted laser desorption ionization time-of-flight mass spectrometry (MALDI-TOF MS) (Figures S1–S33). There was no residual solvent in the obtained viscous liquids after drying under vacuum conditions, which was confirmed by ^{1}H NMR and thermogravimetric analysis (TGA) (*vide infra*). As a note, the yield of **1[2,6-C$_8$C$_{12}$]** (21.2%) was lower than that of the other compounds employed in this study (61–91%).

2.2 Substituent position effect

2.2.1 Phase transition behaviors

It is essential to understand the phase behavior of the alkyl-π FMLs. In our study, the viscosity of alkyl-π FMLs should be evaluated in the isotropic liquid state. Therefore, it is mandatory to determine in which temperature range the synthesized alkyl–DSB compounds are in a thermodynamically stable liquid state. The lower limit of temperature about the isotropic liquid phase for **1[x,y-C$_n$C$_{n+4}$]** regioisomers is judged from the glass transition offset temperature ($T_{g,\,offset}$) or the melting point ($T_{m,\,onset}$). As

shown in Figure 2a, DSC at a 10 °C min^{-1} scan rate resulted from **1[2,4-C$_8$C$_{12}$]** having a complex phase transition behavior, where the transition appeared at −40.7 and −30.9 °C, while the other three regioisomers exhibited a single $T_{g,\,offset}$ at −50.3, −54.5, and −48.6 °C for **1[2,5-C$_8$C$_{12}$]**, **1[2,6-C$_8$C$_{12}$]**, and **1[3,5-C$_8$C$_{12}$]**, respectively. Although their phase transition temperatures appeared much lower than room temperature, some **1[x,y-C$_8$C$_{12}$]** regioisomers unexpectedly crystallized after storage for several weeks at room temperature. We supposed this was a solidification phenomenon seen in SCLs. A simple way to distinguish the supercooling phenomenon is to conduct a heating trace at a relatively slow scan rate of 0.2 °C min^{-1}.[11c] Under the scan rate conditions, the apparent peaks of cold crystallization in **1[2,4-C$_8$C$_{12}$]**, **1[2,5-C$_8$C$_{12}$]**, and **1[3,5-C$_8$C$_{12}$]** were recognized, and the corresponding *crystal*-to-*isotropic* phase transition, $T_{m,\,onset}$, was between 27.4 and 35.4 °C (Figure 2b, Table S1). Additionally, we carried out DSC experiments at a scan rate of 10 °C min^{-1} after annealing **1[x,y-C$_8$C$_{12}$]** regioisomers at −30 °C for 12 h (Figure S34). In this case, the $T_{m,\,onset}$ was different from the one observed in the slower scan rate experiments (Figure 2b). The different crystallization phenomena that occurred due to different thermal histories and/or kinetics are known as typical characteristics of SCLs, in which the nucleation and growth of crystals take place in a metastable SCL phase. Temperature-controlled polarized optical microscopy (POM) experiments can monitor the crystallization process. As a representative example, **1[2,4-C$_8$C$_{12}$]** was investigated under POM at a temperature range of −15 to 50 °C and a heating rate of 0.2 °C min^{-1}. At approximately 1.6 °C, the seeds of crystals appeared and grew further under continuous heating (Figure 2c). Both the DSC and POM results established that **1[2,4-C$_8$C$_{12}$]** formed a crystalline state under precise thermal control. Similarly, **1[2,5-C$_8$C$_{12}$]** and **1[3,5-C$_8$C$_{12}$]** formed a crystalline state at around 25 °C. However, **1[2,6-C$_8$C$_{12}$]** maintained a thermodynamically stable liquid state at a temperature above its $T_{g,\,offset}$ (Figures 2a-b and S34), at least under the monitoring period of up to more than one year of storage at room temperature.

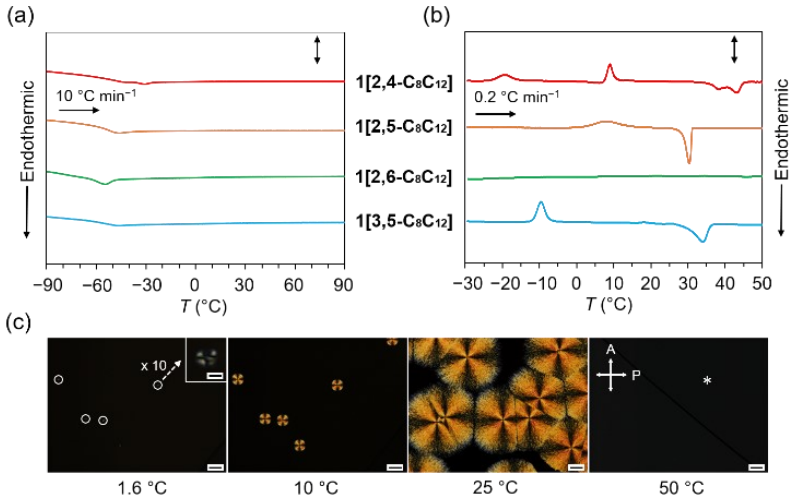

Figure 2. DSC thermograms of **1[2,4-C_8C_{12}]** (red), **1[2,5-C_8C_{12}]** (orange) **1[2,6-C_8C_{12}]** (green), and **1[3,5-C_8C_{12}]** (cyan) under nitrogen flow (a) during the heating scan from −90 to 90 °C at 10 °C min^{-1} (scale bar (sb): 2.0 W g^{-1}); (b) from −30 to 50 °C at 0.2 °C min^{-1} (sb: 1.5 W g^{-1}). (c) POM photographs of **1[2,4-C_8C_{12}]** during heating process (0.2 °C min^{-1}, from −15 °C) at 1.6 °C. (appeared nuclei are denoted with white circles, one of which is magnified (× 10) as an inset indicated by a white dotted arrow, sb: 5 μm), 10 °C, 25 °C, 50 °C. White arrows stand for the transmission axes of the polarizer (P) and analyzer (A), and the asterisk (*) represents the sample area under cross-polarized light, magnification: × 10, sb: 50 μm.

2.2.2 Liquid physical properties

2.2.2.1 Structural analysis

The isotropic phase of four **1[x,y-C_8C_{12}]** regioisomers at 50 °C, judged from the DSC results, was evaluated by POM and SWAXS. There was no birefringence in the POM profiles (Figure S35) or sharp crystalline-like reflection peaks in the SWAXS profiles (Figure 3a). These results indicate that not all **1[x,y-C_8C_{12}]** regioisomers formed long-range ordered structures under the experimental conditions. The SWAXS profiles of the four regioisomers exhibited two broad halos at around 2.6–3.1 and 13.6 nm^{-1} of *q*, which corresponded to the average distances between the π-conjugated DSB moieties and between the molten alkyl chains, respectively. The average DSB–DSB distance judging from the top position of the small angle halo was in the range of 20.6 to 23.9 Å (Table 1). Notably, **1[2,6-C_8C_{12}]** and **1[3,5-C_8C_{12}]** showed an additional halo at 6.1 nm^{-1} of *q* (*d* = 10.3 Å) and a shoulder at 3.9 nm^{-1} of *q* (*d* = 16.1 Å), respectively (Figure 3a). The former one on **1[2,6-C_8C_{12}]** might be explained as the second order

of a rather uniform molecular configuration (size). The four branched alkyl chains at the *ortho*-positions could have covered the central benzene ring of the DSB unit, which enabled it to form a rather packed ellipsoid-like shape (Figure S36a-c). The latter one on **1[3,5-C_8C_{12}]** might be assigned to its small nanoaggregates. This might be due to both branched alkyl chains at the *meta*-positions flipping outward from the DSB unit, which gave rise to possible intermolecular DSB–DSB interactions (Figure S36d).

2.2.2.2 Viscosity

Previous studies on the viscosity of alkyl-π FMLs showed a modulation of the substitution pattern, including the substituent position and alkyl chain length on the π-conjugated molecules, causing an unpredictable tendency in the viscosity. For instance, in alkyloxyphenyl-*N*-methylfulleropyrrolidine liquids, longer linear alkyl chains at the (2,4,6-) substituted positions[3a-b] and branched alkyl chains at the (2,5-) substituted positions[3c] resulted in a lower viscosity. In alkyl–naphthalene liquids[4d] and alkyl–tetrazine liquids,[10] increasing the alkyl chain length led to a higher viscosity due to the enlarged molecular size. In tetrakis(dialkyloxyphenyl)pyrene liquids, a lower viscosity of 6.2 Pa·s was achieved; however, the investigation was carried out with only three different substitution patterns, i.e., at the (3,5-) position with C_6C_{10} or $C_{10}C_{14}$ chains attached and at the (2,5-) position with C_6C_{10} chains attached.[4c] Therefore, the correlation of 'structure–viscosity' for alkyl-π FMLs is still an open question.

Table 1. Summarized SWAXS, complex viscosity (|η*|) and density (ρ) of **1[x,y-C_nC_{n+4}]** and **3[2,5-$C_{10}C_{14}$]** in the solvent-free liquid state

Compound	T (ºC)	$d_{small\ angel\ halo}$ (Å)[a]	$d_{wide\ angel\ halo}$ (Å)[a]	Shoulder (nm^{-1})[b]	|η*| (Pa·s) [c]	ρ (g cm^{-1}) [d]
1[2,4-C_8C_{12}]	50	21.7	4.57	—	0.64	—
	25	—	—	—	2.79	0.919
1[2,5-C_8C_{12}]	50	20.6	4.61	—	0.50	—
	25	—	—	—	2.47	0.904
1[2,6-C_8C_{12}]	50	22.0	4.80	6.1	0.43	—
	25	22.3	4.72	6.1	1.83	0.858
1[3,5-C_8C_{12}]	50	23.9	4.62	3.9	0.94	—
	25	—	—	—	4.06	0.902
1[2,5-C_6C_{10}]	50	19.3	4.63	—	0.65	—
	25	—	—	—	0.40	0.921
1[2,5-$C_{10}C_{14}$]	50	23.8	4.66	—	0.44	—
	25	23.2	4.59	—	1.65	0.899
1[2,5-$C_{12}C_{16}$]	50	24.5	4.59	—	0.50	—
	25	26.5	4.61	—	2.05	0.891
3[2,5-$C_{10}C_{14}$]	50	23.3	4.66	—	0.43	—
	25	23.8	4.59	—	1.59	0.904

[a] Distance (d) was calculated by $d = 2\pi/q$ from the top position of the small- or wide-angle halo. [b] Shoulder was noticed at the typical position. [c] Complex viscosity (|η*|) was determined at an angular frequency (ω) = 10 rad s^{-1}, and strain amplitude (γ) = 0.1. [d] Density (ρ) was measured at 23.7 ± 1.5 °C.

The fluidic behavior of four **1[x,y-C_8C_{12}]** regioisomers was investigated by a rotary rheometer. Their loss viscous moduli (G'') were always higher than the storage elastic moduli (G') throughout the measured angular frequency (ω) (Figure S37). Their complex viscosities (|η*|) were almost independent of the measured ω range, which indicated that they were Newtonian liquids (Figure 3b). As summarized in Table 1, when comparing |η*| between **1[2,4-C_8C_{12}]** with 0.64 Pa·s, **1[2,5-C_8C_{12}]** with 0.50 Pa·s,

and **1[2,6-C$_8$C$_{12}$]** with 0.43 Pa·s or between **1[2,5-C$_8$C$_{12}$]** with 0.50 Pa·s and **1[3,5-C$_8$C$_{12}$]** with 0.94 Pa·s, the branched alkyl chain(s) at the *ortho*-position was more effective for reducing the viscosity than that at the *meta*- and *para*-position. Among the series of **1[x,y-C$_8$C$_{12}$]** regioisomers at 50 °C, **1[2,6-C$_8$C$_{12}$]** exhibited the lowest viscosity and **1[2,5-C$_8$C$_{12}$]** was the second lowest.

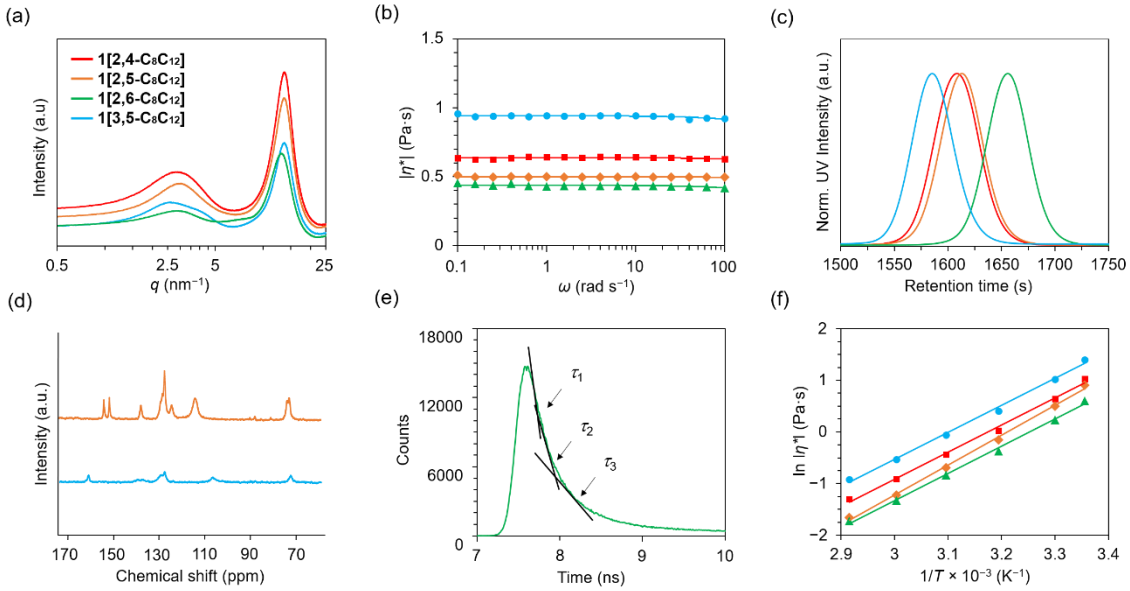

Figure 3. Structural and liquid physical properties of **1[2,4-C$_8$C$_{12}$]** (red), **1[2,5-C$_8$C$_{12}$]** (orange) **1[2,6-C$_8$C$_{12}$]** (green), and **1[3,5-C$_8$C$_{12}$]** (cyan). (a) SWAXS profiles at 50 °C. (b) $|\eta^*|$ as a function of ω, with γ = 0.1 at 50 °C. (c) The normalized chromatograms are indicated by an ultraviolet (UV) detector in GPC by using chloroform as eluent at room temperature. (d) Solid-state ^{13}C NMR spectra of **1[2,5-C$_8$C$_{12}$]** (orange) and **1[3,5-C$_8$C$_{12}$]** (cyan) in the solvent-free liquid state at approximately 40 °C. (e) In the positron decay curve of **1[2,6-C$_8$C$_{12}$]** by the PSA, three decay lifetime components (τ_1, τ_2, τ_3) were indicated by their slops. (f) Arrhenius plots of ln $|\eta^*|$ against $1/T$ for the measured temperature from 25 °C to 70 °C.

The viscosity of various fluids, including molten polymers[15] and ionic liquids (ILs),[16] can be determined by multiple factors, such as the size and motion of liquid molecules, fractional free volume, density, temperature, and pressure.[15-18] In the present alkyl–DSB liquids, we focused on the microscopic molecular parameters,

specifically the molecular size, molecular motion, and fractional free volume for their contribution to the viscosity.

We studied the molecular size of the alkyl–DSBs by GPC in monitoring its retention time (t_R). Chromatograms showed that t_R was in the order of **1[3,5-C_8C_{12}]** < **1[2,4-C_8C_{12}]** < **1[2,5-C_8C_{12}]** < **1[2,6-C_8C_{12}]** (Figures 3c and S38a, Table S2). The longer t_R reflected a smaller hydrodynamic volume of the molecules. From this viewpoint, **1[2,6-C_8C_{12}]** formed the smallest molecular size (configuration), and **1[3,5-C_8C_{12}]** had the largest one. This agreed well with their different $|\eta^*|$ obtained in the solvent-free liquid state at 50 °C, even though the molecular size was determined in a monomerically dispersed chloroform solution.

Next, we considered the effect of the molecular motions (translational and rotational motions). According to the Stokes–Einstein equation, $\eta = kT\tau_c/4\pi a^3$, where k, T, τ_c, and a are the Boltzmann's constant, absolute temperature, correlation time, and radius of the molecule, respectively, the lower viscosity was achieved by a shorter τ_c, which means faster molecular motions. SSNMR can investigate molecular motion in the solvent-free liquid state,[19] albeit typically used for solid substances, which was previously applied in the case of alkyl–pyrene liquids[4c] and alkyl–porphyrin liquids.[5a] As reported, the dipolar decoupling/magic angle spinning (DD/MAS) mode in SSNMR provides information about molecular motion in the range of 10^{-5} to 10^{-7} s. Judging from their viscosity values, this method should be suitable for alkyl–DSB liquids. As representative regioisomers, **1[2,5-C_8C_{12}]** and **1[3,5-C_8C_{12}]** were measured in the DD/MAS mode at approximately 40 °C. The ^{13}C NMR spectrum of **1[2,5-C_8C_{12}]** exhibited better-resolved and more intensive peaks than those of **1[3,5-C_8C_{12}]** at the same carbons of the central phenyl ring or vinylene units (Figure 3d). The results indicated that **1[2,5-C_8C_{12}]** had faster molecular motions than **1[3,5-C_8C_{12}]**, which was in good agreement with the relative $|\eta^*|$ found in these two regioisomers.

The contribution from the free volume and/or fractional free volume was investigated by PSA. As explained in the Doolittle equation, $\eta = A\exp(BV_0/V_f)$, where A or B, V_0, and V_f are simulated constants, occupied volume, and free volume, respectively. The equation is sometimes expressed as $\eta = A\exp(B/f)$, where $f = V_f/V$, and $V = V_f + V_0$; f and V are the fractional free volume and specific volume, respectively. If we consider that $V_0 >> V_f$, this can be rewritten as $\eta = A\exp(BV_0/V_f)$. In this case, the lower viscosity resulted from a larger V_f or more precisely, a larger $f \approx V_f/V_0$.[18a-d]

In the alkyl–DSB liquid case, the free volume refers to the unoccupied intra- and/or intermolecular space. Therefore, a sufficient free volume allows the molecules to move into the neighboring void with less friction.[18d] Positron annihilation can provide the characteristics of the free volume and fractional free volume in condensed matter; the decay of the positron is usually divided into three lifetime components (τ_1, τ_2, and τ_3), and their relative intensities (I_1, I_2, and I_3) are also provided.[20a-d] The fractional free volume expressed as I_3 is the one commonly discussed for the contribution to the viscosity of fluids.[20e-f] Two representative regioisomers, **1[2,6-C_8C_{12}]** and **1[3,5-C_8C_{12}]**, were characterized by PSA using radiation from a ^{22}Na nuclear source. **1[2,6-C_8C_{12}]** exhibited a τ_3 of 2.866 ± 0.012 ns with a I_3 of 26.98 ± 0.13% (Figure 3e), which was longer and a larger portion than that of **1[3,5-C_8C_{12}]** with a τ_3 of 2.833 ± 0.012 ns and a I_3 of 23.38 ± 0.11% (Figure S38b, Table S3). The results indicated that the larger fractional free volume of **1[2,6-C_8C_{12}]** lowered its viscosity.

In addition, the density (ρ) is a valid value for comparing the free volume. The specific volume of a molecular system (reciprocal of density, $1/\rho$) is composed of V_0 and V_f.[18b-c] If V_0 is considered to be independent of the temperature,[18c] which is nearly equivalent to the relative molecular size determined from GPC, the trend of the free volume can be estimated by $V_f = 1/\rho - V_0$. The density of the **1[x,y-C_8C_{12}]** regioisomers is summarized in Table 1. We realized that **1[2,6-C_8C_{12}]** exhibited a smaller density than **1[3,5-C_8C_{12}]**. It is similar to reported ILs with curled ether-substituted ammonium cations in that the density was determined by the free volume and molecular size.[21] To sum up, the larger fractional free volume in the **1[x,y-C_8C_{12}]** regioisomers exhibited a smaller viscosity, particularly in **1[2,6-C_8C_{12}]**.

We examined the various aspects of the influential factors on the viscosity for the **1[x,y-C_8C_{12}]** regioisomers and found that some were highly correlated with each other. For instance, both the molecular size (hydrodynamic radius, a) and molecular motion (correlation time, τ_c) are involved in the Stokes–Einstein equation. The Doolittle equation includes the molecular size and free volume. Through our investigations, at least we could conclude that the smaller molecular size, faster molecular motion, and larger fractional free volume resulted in a lower viscosity of the alkyl–DSB liquids.

Temperature is also a significant factor for determining the viscosity (Table S4). In the Arrhenius equation, the viscosity is expressed as $\eta = a \exp(E_a/RT)$, where a, E_a, R, and T are a constant, the activation energy for viscous flow, gas constant, and the

absolute temperature, respectively.[18h-i] When E_a/R is expressed as a constant, b, the equation can be written as $\eta = a \exp(b/T)$ and rewritten as $\ln \eta = \ln a + b/T$. Arrhenius plots of $\ln |\eta^*|$ against $1/T$ for the four regioisomers fit well with a linear fitting parameter (r^2) close to 1 (Figure 3f, Table S5). Their E_a was calculated from the slopes as 43.6, 48.1, 43.7, and 43.4 kJ mol^{-1}, respectively. **1[2,5-C$_8$C$_{12}$]** showed a slightly larger E_a than the other three regioisomers. Therefore, **1[2,5-C$_8$C$_{12}$]** was a rather sensitive compound under temperature variations. In addition, their E_a was comparable to that of reported polymer fluids such as the molten state of low-density polyethylene,[22a] poly(ethylene oxide–ethylene carbonate),[22b] and polyphenylene sulfide,[22c] while higher than typical ILs[22d-e] such as [1-butyl-3-methylimidazolium][BF_4] analyzed with the Arrhenius model.

2.2.3 Optical properties

Our main focus on the optical properties of **1[x,y-C$_8$C$_{12}$]** regioisomers, having bulky and long branched alkyl chains, was whether the monomeric optical properties, e.g. absorption and fluorescence wavelengths, of the DSB core unit in the solution state could be maintained in the solvent-free liquid state.

2.2.3.1 Light absorption and fluorescent properties

To have a clearer understanding of the substituent position effect, the optical properties of the four regioisomers were explored. UV-Vis absorption and fluorescence spectroscopy measurements of the **1[x,y-C$_8$C$_{12}$]** regioisomers in the solvent-free liquid state and in dichloromethane (CH_2Cl_2) solution were conducted and their optical properties were summarized (Table S6). There was no significant difference in the absorption and fluorescence features between **1[2,4-C$_8$C$_{12}$]**, **1[2,5-C$_8$C$_{12}$]**, and **1[2,6-C$_8$C$_{12}$]** in the solvent-free liquid/SCL state and CH_2Cl_2 solution, as shown in Figure 4a. This indicated that the DSB chromophore of the three regioisomers had not aggregated with neighboring molecules in the solvent-free liquid/SCL state as appeared in their spectra like CH_2Cl_2 solution, where the molecules were monomerically dispersed. This might be due to at least one branched alkyl chain at the *ortho*-position being bulky enough to prevent π–π interactions among the DSB chromophores in the solvent-free liquid state. In contrast, **1[3,5-C$_8$C$_{12}$]** showed a 24 nm wider full width at half maximum (FWHM) of the UV-Vis absorption spectrum and

a 3 nm red-shifted fluorescence spectrum in the solvent-free liquid state compared to that in the CH_2Cl_2 solution (Figure 4a). This indicated the existence of interactions among neighboring DSB units of **1[3,5-C_8C_{12}]**. In the film state of unsubstituted DSB[23a] and 1,4-bis(3,5-dimethoxystyryl)benzene compounds,[23b] their absorption and fluorescence peaks broadened and shifted significantly to a longer wavelength about 50 nm from those observed in the dilute solution. Therefore, **1[3,5-C_8C_{12}]** in the solvent-free SCL state involved only weak π–π interactions. In addition, the optical properties of three solid samples formed from their SCL states except **1[2,6-C_8C_{12}]** were investigated (Figure S39a-c). Their UV-Vis absorption and fluorescence spectra showed apparent 6–11 and 4–9 nm red shifts, respectively, compared to those in the solvent-free SCL state (Table S6). The Commission internationale de l'éclairage (CIE) values in the solid state evidently changed from their solvent-free SCL state as well (Figure 4b). Therefore, a thermodynamically stable liquid at room temperature is a prerequisite for consistent optical functions.

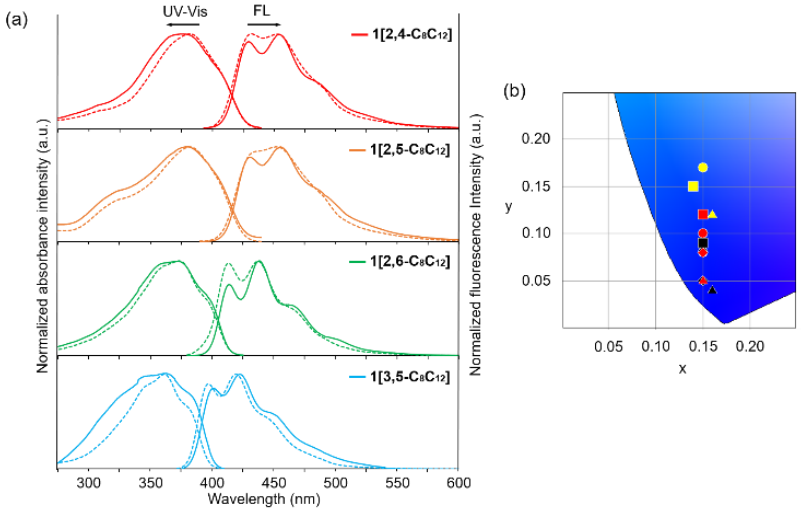

Figure 4. (a) The normalized UV-Vis absorption and fluorescence spectra of **1[2,4-C_8C_{12}]** (red), **1[2,5-C_8C_{12}]** (orange), **1[2,6-C_8C_{12}]** (green), and **1[3,5-C_8C_{12}]** (cyan) in the solvent-free liquid state (solid lines) and CH_2Cl_2 solution (dashed lines, UV-Vis: 10 μM; fluorescence: 0.2 μM), respectively. (b) A part of the Commission internationale de l'éclairage (CIE) chromaticity diagram for **1[2,4-C_8C_{12}]** (circle), **1[2,5-C_8C_{12}]** (square), **1[2,6-C_8C_{12}]** (rhombus), and **1[3,5-C_8C_{12}]** (triangle) in the solvent-free liquid state (red), CH_2Cl_2 solution (black), and solid state (yellow), respectively. The black circle and black rhombus are overlapped with a black square.

Here, we looked into the details of the substitution position effect in the UV-Vis absorption and fluorescence spectra for each regioisomer in the solvent-free liquid and CH_2Cl_2 solution state. We observed clearer vibronic features in the fluorescence compared with their absorption spectra (Figure 4a), which could be explained by the photoexcited DSB molecules becoming less twisted than in the ground state.[14] The fluorescence spectra of **1[2,6-C_8C_{12}]** and **1[3,5-C_8C_{12}]** in the CH_2Cl_2 solution state with a symmetric substitution pattern had clear vibronic bands compared to the spectra of **1[2,4-C_8C_{12}]** and **1[2,5-C_8C_{12}]**, where the substitution pattern was asymmetric. Those broader and smoother spectra with almost vanished vibronic sub-bands in **1[2,4-C_8C_{12}]** and **1[2,5-C_8C_{12}]** might be due to their greater torsional flexibility.[14] Another hypothesis was the 'rotamer effect' resulting from the unrestricted single C–C bond rotation between the vinylene unit and the terminal phenyl ring, and each rotamer might have exhibited a different degree of conjugation.[4c, 24]

Fluorescence quantum yield (FL-QY) and fluorescence lifetime measurements were carried out to investigate the **1[x,y-C_8C_{12}]** regioisomers in the excited state. The four regioisomers in the CH_2Cl_2 solution showed absolute FL-QY in the range of 0.74–0.95 as reported in alkyl–DSB liquids.[4a] In the solvent-free liquid state, their FL-QY decreased to some extent (Table S7), which might have resulted from the increased nonradiative decay rate constant (k_{NR}) and decreased radiative decay constant (k_R), because the intermolecular vibrational energy transfer between the same molecules takes place more efficiently than that between the molecular solute and solvent. It is worth noting that **1[2,5-C_8C_{12}]** had a larger amplitude-weighted average lifetime (τ_{ave}) than the other regioisomers in both the CH_2Cl_2 solution (1.68 ns) and the solvent-free liquid state (1.21 ns), which indicated that it stayed longer in the excited state before emitting a photon to its ground state (Figure S40).

2.2.3.2 Theoretical calculation

Density functional theory (DFT) calculations at the B3LYP/6-31G(d,p) level were conducted to gain insight into the substituent position effect on the molecular configuration as well as the electronic structures. The energy-minimized geometries were obtained for methoxy-appended **2[x,y-CH_3]** regioisomers as the simplest model. The substantial dihedral angles θ_1 and θ_2 (in Figure S41) could indicate the nonplanarity of the DSB, except for **2[3,5-CH_3]**. Notably, **2[2,4-CH_3]** and **2[2,5-CH_3]**

show a similar twisted structure where θ_1 and θ_2 are around 15° and 6°, respectively, and **2[2,6-CH_3]** consists of a smaller θ_1 of 6.4° and a larger θ_2 of 7.5° (Figure S41, Tables S8–S11). Although the alkyl chain at the *ortho*-position has the largest steric hindrance, the maintained molecular planarity might be influenced by the hydrogen bond between the oxygen atom of the alkoxy group and the hydrogen atom on the nearby vinylene unit.[14a] We have studied the effect of alkoxy groups on the different substituent positions for their electronic structures, including the highest occupied molecular orbital (HOMO), the lowest unoccupied molecular orbital (LUMO), and the HOMO–LUMO energy gap (E_g) (Figure S42).[25] The electron-donating ability of alkyloxy groups generally raises the HOMO and LUMO energy levels.[25] In contrast, the decreased degree of planarity induced by steric hindrance brought about decreasing HOMO and increasing LUMO energies, resulting in a wider E_g.[13a] The results indicated that the electron-donating ability of the alkyloxy groups was contributing more to the increased HOMO energies of **2[x,y-CH_3]** regioisomers. Time-dependent (TD)-DFT calculations were also conducted to determine the first excited-state transition to support a further understanding of the substituent position effect. Although the calculated absorption λ_{max} was relatively larger than the experimental results (Figure 4a), the tendency of the calculated oscillator strengths almost agreed with that of the experimental molar absorption coefficients (Figure S43, Table S12).

2.2.4 Thermal- and photo-stabilities

Better thermal- and photo-stabilities of alkyl-π FMLs are always beneficial for consistent performance in optoelectronic devices. The thermal stability of alkyl-π FMLs can be represented by their thermal decomposition temperature ($T_{d95\%}$) in TGA. The $T_{d95\%}$ was in the order of **1[3,5-C_8C_{12}]** > **1[2,4-C_8C_{12}]** ≥ **1[2,5-C_8C_{12}]** >> **1[2,6-C_8C_{12}]** (Figure 5a, Table S1). **1[2,6-C_8C_{12}]** exhibited a $T_{d95\%}$ at 215 °C, while the other three regioisomers showed a $T_{d95\%}$ above 380 °C. The lower thermal stability of **1[2,6-C_8C_{12}]** might be due to the larger steric hindrance of the four branched alkyl chains at the *ortho*-position (Figure S36c).

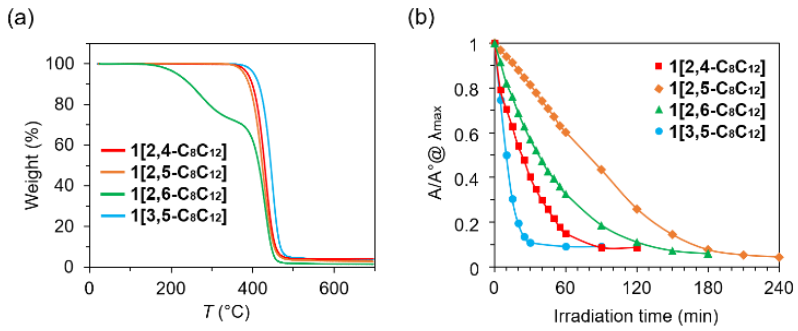

Figure 5. (a) TGA graph at a heating rate of 10 °C min^{-1} from room temperature to 700 °C under argon flow. (b) In photostability studies, the variation of absorbance λ_{max} in CH_2Cl_2 solution was monitored by UV-Vis absorption spectroscopy after Xenon lamp irradiation. **1[2,4-C_8C_{12}]** (red, square), **1[2,5-C_8C_{12}]** (orange, rhombus), **1[2,6-C_8C_{12}]** (green, triangle), and **1[3,5-C_8C_{12}]** (cyan, circle).

Photodegradation under continuous light irradiation reflects the photostability of the **1[x,y-C_8C_{12}]** regioisomers. It is known that DSB compounds are sensitive to singlet oxygen and irradiation conditions depending upon their substitution pattern.[26a] Absorbance at λ_{max} of the UV-Vis spectra was monitored as a function of the irradiation time using a Xenon lamp.[4b,26] The absorbance λ_{max} of **1[3,5-C_8C_{12}]** decreased to half the intensity within 10 min, while **1[2,5-C_8C_{12}]** reached the half intensity up to 78 min. **1[2,5-C_8C_{12}]** exhibited even better stability than **1[2,6-C_8C_{12}]** (Figure 5b). The photostability of the **1[x,y-C_8C_{12}]** regioisomers was thought to be contributed mainly from two important factors: the protected effectiveness of a π-conjugated unit by branched alkyl chains and the photoreactivity of the π-conjugated unit. We tried using Raman spectroscopy to obtain chemical structural information relevant to the photostability. The detailed Raman assignment of four regioisomers as well as their frequency calculations are provided in the Supplementary Information (Figures S44–S47, Table S13).[27] The protected effectiveness of π-conjugated units could be mainly considered from their steric hindrance in the vicinity of the vinylene C–H bonds, which is basically reflected in the relative frequency of the corresponding bending motions. If the hydrogen atom hits other obstacles during the bending motion, it will move back to the equilibrium position earlier and exhibit a larger frequency.[27g] The frequency trend of vinylene C–H bonds **1[3,5-C_8C_{12}]** (1313 cm^{-1}) < **1[2,5-C_8C_{12}]** (1316 cm^{-1}) – **1[2,4-C_8C_{12}]** (1317 cm^{-1}) < **1[2,6-C_8C_{12}]** (1329 cm^{-1}) indicated that the alkyl chain at

the *ortho*-position had a larger steric hindrance compared with that at the *meta*- or *para*-position, which would be more valid for enhancing the photostability. It is an experimental fact that **1[2,5-C_8C_{12}]** was more photostable than **1[2,6-C_8C_{12}]** (Figure 5b), although **1[2,6-C_8C_{12}]** had the largest steric hindrance around the vinylene C–H bonds. We presume that the terminal phenyl rings of **1[2,6-C_8C_{12}]** were less protected by the alkyl chains at the *ortho*-position, which were both directed inwards to the central phenyl ring (Figure S36c). A singular finding in the Raman spectrum of **1[2,6-C_8C_{12}]** was the distortion of the terminal phenyl rings, as the phenyl CC stretch band was split by 10 cm^{-1} (Figure S44). This could also be related to its lower photostability compared to that of **1[2,5-C_8C_{12}]**.

In a summary of the substituent position effect, although the optical properties of each regioisomer were altered to some extent, except for **1[3,5-C_8C_{12}]**, the other three regioisomers maintained their absorption and fluorescence features in the solvent-free liquid state. **1[2,6-C_8C_{12}]** had the lowest viscosity as a thermodynamically stable liquid at room temperature and it exhibited a relatively low thermal stability, while **1[2,5-C_8C_{12}]** had better thermal- and photo-stabilities, and the second lowest viscosity. Therefore, further investigations on the alkyl chain length effect were conducted on the **1[2,5-C_nC_{n+4}]** compounds.

2.3 Alkyl chain length effect

Regulation of the alkyl chain length on π-conjugated molecules is an effective method for tuning the intermolecular interactions, self-assembled structures, and optoelectronic properties.[28] The effect of the alkyl chain length has been seen not only in cases of crystalline or liquid crystalline materials, but also in alkyl-π FMLs. Changing the length of the alkyl chains on an alkyl-π FML can control the balance of intermolecular forces between the π–π interactions of the π-conjugated molecules and the van der Waals interactions governed by the alkyl chains. Their viscosity,[4d] phase transition temperatures,[11] and optoelectronic properties[5a, 11] are not monotonically and complicated so they are sensitive to the chemical structures of alkyl-π FMLs.

2.3.1 Thermal and optical properties

The effect of the alkyl chain length on the thermal properties for **1[2,5-C$_n$C$_{n+4}$]** compounds was investigated in terms of their phase transition behaviors and thermal stability. When shorter C_6C_{10} chains were attached, **1[2,5-C$_6$C$_{10}$]** exhibited a $T_{g,\,offset}$ at −50.5 °C, which was close to that of **1[2,5-C$_8$C$_{12}$]**. When the alkyl chains were lengthened to $C_{10}C_{14}$ or $C_{12}C_{16}$, their phase transition temperature increased. The $T_{g,\,offset}$ of **1[2,5-C$_{10}$C$_{14}$]** appeared at −39 °C, and **1[2,5-C$_{12}$C$_{16}$]** exhibited a dominant sharp $T_{m,\,onset}$ at −23.3 °C and a minor one at 3.9 °C (Figure 6a, Table S1). The highest $T_{m,\,onset}$ of **1[2,5-C$_{12}$C$_{16}$]** was derived from the dominant van der Waals interactions among the longest $C_{12}C_{16}$ chains.

We conducted DSC investigations with a relatively slow scan rate at 0.2 °C min^{-1} to discriminate whether the obtained liquids were in a thermodynamically stable state or a kinetically trapped SCL state (Figure 6b). **1[2,5-C$_6$C$_{10}$]** showed a broad T_c at 21.0 °C and a clear $T_{m,\,onset}$ at 32.3 °C, while no phase transition was observed on **1[2,5-C$_{10}$C$_{14}$]** and **1[2,5-C$_{12}$C$_{16}$]** under this condition. Annealing of 12 h was applied at −30 °C for **1[2,5-C$_6$C$_{10}$]** and **1[2,5-C$_{10}$C$_{14}$]** and at 0 °C for **1[2,5-C$_{12}$C$_{16}$]**, respectively, and the following heating scan was performed at 10 °C min^{-1}. Under such conditions, whereas **1[2,5-C$_6$C$_{10}$]** and **1[2,5-C$_{10}$C$_{14}$]** did not show any phase transition, **1[2,5-C$_{12}$C$_{16}$]** exhibited a *crystalline*-to-*isotropic* liquid phase transition ($T_{m,\,onset}$ at 11.2 °C), which was a sign that the crystallization proceeded during the low-temperature annealing (Figure 6c). These results suggested that **1[2,5-C$_{10}$C$_{14}$]** and **1[2,5-C$_{12}$C$_{16}$]** formed a thermodynamically stable liquid state at room temperature. As discussed for **1[x,y-C$_8$C$_{12}$]**, at 50 °C all the **1[2,5-C$_n$C$_{n+4}$]** compounds exhibited an isotropic liquid phase, and this temperature was also used for other analyses. The TGA results showed that all the **1[2,5-C$_n$C$_{n+4}$]** compounds had similar thermal stabilities with $T_{d95\%}$ above 375 °C, indicating that the effect of the alkyl chain length was less significant (Figure S48).

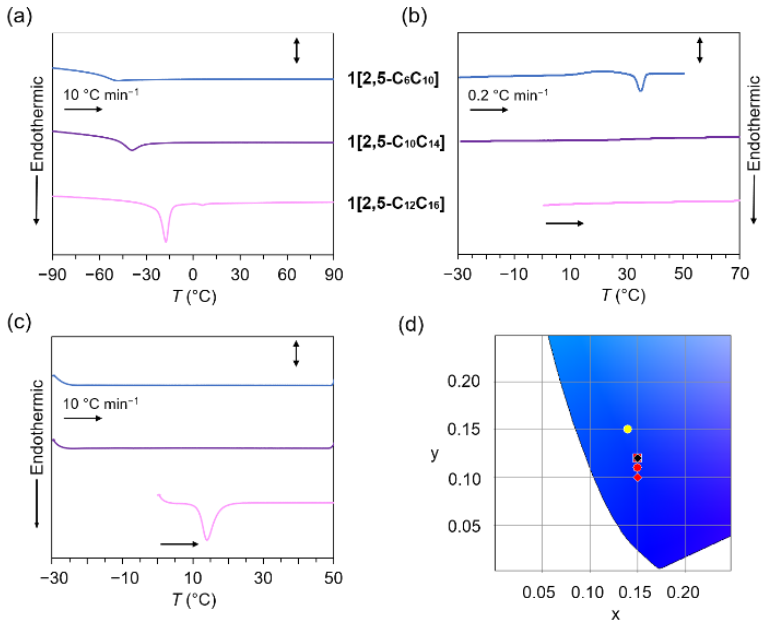

Figure 6. DSC thermograms of **1[2,5-C$_6$C$_{10}$]** (blue), **1[2,5-C$_{10}$C$_{14}$]** (purple), and **1[2,5-C$_{12}$C$_{16}$]** (pink) at the heating scan (a) from −90 to 90 °C at 10 °C min^{-1} (sb: 2.0 W g^{-1}); (b) **1[2,5-C$_6$C$_{10}$]** from −30 to 50 °C; **1[2,5-C$_{10}$C$_{14}$]** from −30 to 70 °C; **1[2,5-C$_{12}$C$_{16}$]** from 0 to 70 °C at 0.2 °C min^{-1} (sb: 1.5 W g^{-1}); (c) **1[2,5-C$_6$C$_{10}$]** and **1[2,5-C$_{10}$C$_{14}$]** were heated from −30 to 50 °C with 10 °C min^{-1} after annealing at −30 °C for 12 h. **1[2,5-C$_{12}$C$_{16}$]** was heated from 0 to 70 °C with 10 °C min^{-1} after annealing at 0 °C for 12 h (sb: 2.0 W g^{-1}). (d) A part of CIE chromaticity diagram of **1[2,5-C$_6$C$_{10}$]** (circle), **1[2,5-C$_{10}$C$_{14}$]** (square), **1[2,5-C$_{12}$C$_{16}$]** (rhombus) in the solvent-free liquid state (red), CH_2Cl_2 solution (black), and solid state (yellow), respectively. The red square is overlapped with a black circle, a black square, and a black rhombus.

All the **1[2,5-C$_n$C$_{n+4}$]** compounds exhibited similar UV-Vis absorption and fluorescence spectra in the solvent-free liquid state and CH_2Cl_2 solution (Figure S49). Their CIE values in the CH_2Cl_2 solution were almost identical, and that in the solvent-free liquid state indicated a similar luminescence color. (Figure 6d, Table S6). Moreover, no significant differences were observed in their fluorescence lifetime decay profiles (Figure S50) as well as in the Fourier-transform infrared spectroscopy spectra (Figure S51). Raman bands of alkyloxy groups were also negligible in the spectra, as indicated by the similarity between **1[2,5-C$_8$C$_{12}$]** and **1[2,5-C$_{10}$C$_{14}$]** in the solvent-free liquid state (Figure S44). The above results indicated that the effect of the alkyl chain

length in **1[2,5-C$_n$C$_{n+4}$]** was not predominant on the electronic structure of the DSB unit, and thus not on the optical properties either.

We further investigated the optical properties of a kinetically trapped SCL sample, **1[2,5-C$_6$C$_{10}$]**, in the solidified state (Figure S39d). The UV-Vis absorption spectra in the solid state exhibited a 6 nm red-shifted absorbance λ_{max} compared with those in the solvent-free liquid state (Table S6). This indicated that there could be a certain molecular arrangement like the formation of *J*-aggregation of the DSB units,[14d] which was distinct from *H*-aggregation in unsubstituted crystalline DSB.[14e] The fluorescence spectrum and CIE value in the solid state also red-shifted to a longer wavelength (increased *y*-score, Figure 6d), which could be explained by an increased molecular organization or some contribution from the reabsorption of fluorescence at a shorter wavelength region. The FL-QY of the solid sample was relatively larger than that in the solvent-free liquid state and smaller than that in the CH_2Cl_2 solution (Table S7), which showed the same tendency as other reported alkyl-π SCLs.[11] This could be understood by their different types of nonradiative decay. In this case, the optical properties of **1[2,5-C$_6$C$_{10}$]** changed after solidification from the SCL state at room temperature.

2.3.2 Liquid physical properties

The amorphous and fluidic nature of **1[2,5-C$_n$C$_{n+4}$]** compounds at 50 °C was evaluated by POM (Figures S35b and S52a-c), SWAXS (Figures 3a and S53), and rheology (Figures S37b and S54). The larger G'' than G' and independent $|\eta^*|$ as a function of the measured ω (Figure S55a) indicated that they were Newtonian-type liquids. It is noteworthy that we found a minimum viscosity at the alkyl chain length of $C_{10}C_{14}$. As shown in Figure 7a, the $|\eta^*|$ of **1[2,5-C$_6$C$_{10}$]**, 0.65 Pa·s, was greater than that of **1[2,5-C$_8$C$_{12}$]**. When the alkyl chains were lengthened from C_8C_{12} to $C_{10}C_{14}$, the $|\eta^*|$ of **1[2,5-C$_{10}$C$_{14}$]** decreased to 0.44 Pa·s. In contrast, when attaching further longer alkyl chains to $C_{12}C_{16}$, the $|\eta^*|$ of **1[2,5-C$_{12}$C$_{16}$]** increased to 0.50 Pa·s. Previous studies found two trends in the viscosity as a function of the alkyl chain length. Alkyl–fullerene,[3] alkyl–anthracene,[11c] and alkyl–pyrene[4c] liquids exhibited a decreasing viscosity with increasing alkyl chain length, while alkyl-π liquids composed of naphthalene[4d] and tetrazine[10] showed an increasing viscosity with increasing alkyl chain length. Therefore, the effect of the alkyl chain length on the DSB system was rather complex.

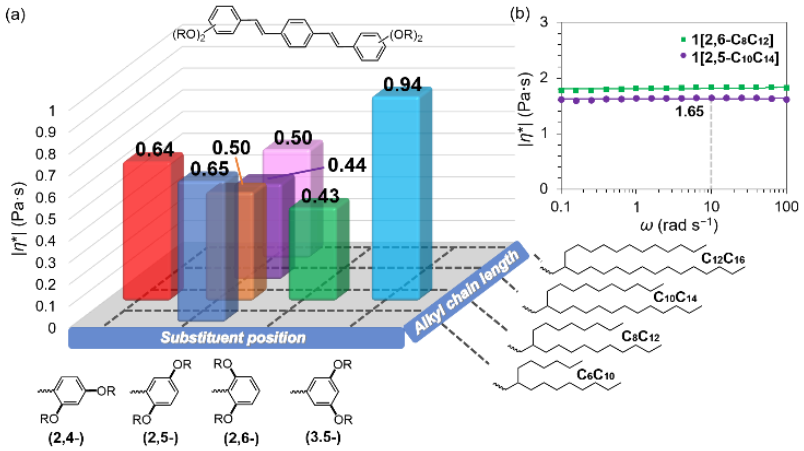

Figure 7. Complex viscosity ($|\eta^*|$) of (a) **1[2,4-C$_8$C$_{12}$]** (red), **1[2,5-C$_8$C$_{12}$]** (orange), **1[2,6-C$_8$C$_{12}$]** (green), **1[3,5-C$_8$C$_{12}$]** (cyan), **1[2,5-C$_6$C$_{10}$]** (blue), **1[2,5-C$_{10}$C$_{14}$]** (purple), and **1[2,5-C$_{12}$C$_{16}$]** (pink) as a function of ω, with γ = 0.1 at 50 °C; (b) of **1[2,6-C$_8$C$_{12}$]** (green, square) and **1[2,5-C$_{10}$C$_{14}$]** (purple, circle) as a function of ω, with γ = 0.1 at 25 °C in the solvent-free liquid state.

The molecular sizes of the **1[2,5-C$_n$C$_{n+4}$]** compounds were similarly determined as for the **1[x,y-C$_8$C$_{12}$]** regioisomers by GPC (Figure S56). The gradually decreased t_R from **1[2,5-C$_6$C$_{10}$]** to **1[2,5-C$_{12}$C$_{16}$]** reflected the enlarged molecular size (Table S2). The smallest molecular size of **1[2,5-C$_6$C$_{10}$]** did not bring the lowest viscosity, which differed from the trend seen at different substituent positions. Therefore, apart from the crucial factors on the viscosity studied for the **1[x,y-C$_8$C$_{12}$]** regioisomers, the content ratio of the alkyl chains and π-conjugated moiety, as well as the van der Waals interactions on the alkyl chains, would play a more important role in the 'structure–viscosity' relationship. When the alkyl chains were lengthened from C_6C_{10} to $C_{12}C_{16}$, the alkyl chain content ratio based on the molecular weight in the compound increased from 77.6% to 88.5%. As seen in the refractive index (RI), their values decreased with the increasing alkyl chain length (Table 1), which might be due to the gradually decreased density of the π-electrons.[23c] In the isotropic liquid state, the **1[2,5-C$_n$C$_{n+4}$]** compounds possessing longer alkyl chains could have a larger entropy governed by the molten alkyl chains. Nevertheless, the longest alkyl chains, $C_{12}C_{16}$, could have led to enhanced van der Waals interactions, which prevailed over the entropy contribution to the viscosity. In the temperature-dependent viscosity analysis of **1[2,5-C$_n$C$_{n+4}$]**

compounds, a linear correlation was observed in the Arrhenius plots for ln |η^*| against 1/T (Figure S55b).[22] Their E_a calculated from each slope was 45.2 (n = 6), 39.2 (n = 10), and 42.2 (n = 12) kJ mol^{-1} (Table S5). Compared with the above **1[x,y-C_8C_{12}]** regioisomers, **1[2,5-$C_{10}C_{14}$]** exhibited the lowest E_a, which indicated that it was most insensitive under the varied temperature range and had the lowest viscosity among the alkyl–DSB liquids. It is noted that at 50 °C, the |η^*| of **1[2,6-C_8C_{12}]** was the lowest among all the **1[x,y-C_nC_{n+4}]** compounds (Figure 7a), whereas at 25 °C, **1[2,5-$C_{10}C_{14}$]** scored a lower viscosity (1.65 Pa·s) than that of **1[2,6-C_8C_{12}]** (1.83 Pa·s) (Figure 7b).

In brief, a superior DSB liquid can be specified through investigations on the effect of the substituent position and alkyl chain length. The 2-decyltetradecyloxy group at the 2,5-substituted position (2,5-$C_{10}C_{14}$) is the substitution pattern for the DSB system to achieve the lowest viscosity at room temperature. Furthermore, the attached 2,5-$C_{10}C_{14}$ substitution pattern did not affect the optical properties of the DSB core unit in the solvent-free liquid state.

2.4 Applicability of 2,5-$C_{10}C_{14}$ substitution pattern on dicyanostyrylbenzene

To enrich the usefulness of the 2,5-$C_{10}C_{14}$ substitution pattern for the DSB-type compound, a dicyanostyrylbenzene (DCS) attracted our attention. The introduction of cyano groups on the vinylene C=C bonds of the DSB molecules results in enlarged π-conjugation with a higher molecular coplanarity, so that the DCS exhibits more pronounced π–π interactions than the DSB. Moreover, the electron-withdrawing characteristic of the cyano group reflects its optical properties. As reported, DCS compounds with different substitution patterns exhibited several luminescent properties, such as excimer formation,[29a] mechanochromic luminescence,[29b] and solid-state luminescence enhancement.[29c] Therefore, DCS would be a candidate for testing the applicability of the 2,5-$C_{10}C_{14}$ substitution pattern for designing superior luminescent alkyl-π FMLs. **3[2,5-$C_{10}C_{14}$]** was synthesized by Knoevenagel reaction[29d] in an acceptable yield of 67% and was obtained as a viscous liquid at room temperature (Scheme S4, Figure 8b). The thermal, liquid physical and optical properties of **3[2,5-$C_{10}C_{14}$]** are discussed below. TGA indicated that it is thermally stable at temperatures up to around 380 °C ($T_{d95\%}$) (Figure S57a). Although one broad crystallization peak appeared on the cooling curve, multiple melting peaks from −39.8 to −9.7 °C in DSC were observed on the heating curve at 10 °C min^{-1} (Figure 8c).

When the scan rate was slowed down to 5 or 2.5 °C min^{-1}, the multiple melting peaks became less apparent, but were still far away from 25 °C (Figure S57b). Therefore, **3[2,5-C$_{10}$C$_{14}$]** is a thermodynamically stable liquid at room temperature. The SWAXS profile of **3[2,5-C$_{10}$C$_{14}$]** at 25 °C exhibited only two broad halos, which proved that there was no long-range ordered structure (Figure 8d). Importantly, **3[2,5-C$_{10}$C$_{14}$]** was also a Newtonian liquid, indicated by the independent |η*| in the measured ω range (Figure 8e). The |η*| of **3[2,5-C$_{10}$C$_{14}$]** achieved 1.59 Pa·s at 25 °C, which was lower than that of **1[2,5-C$_{10}$C$_{14}$]** (Table S4).

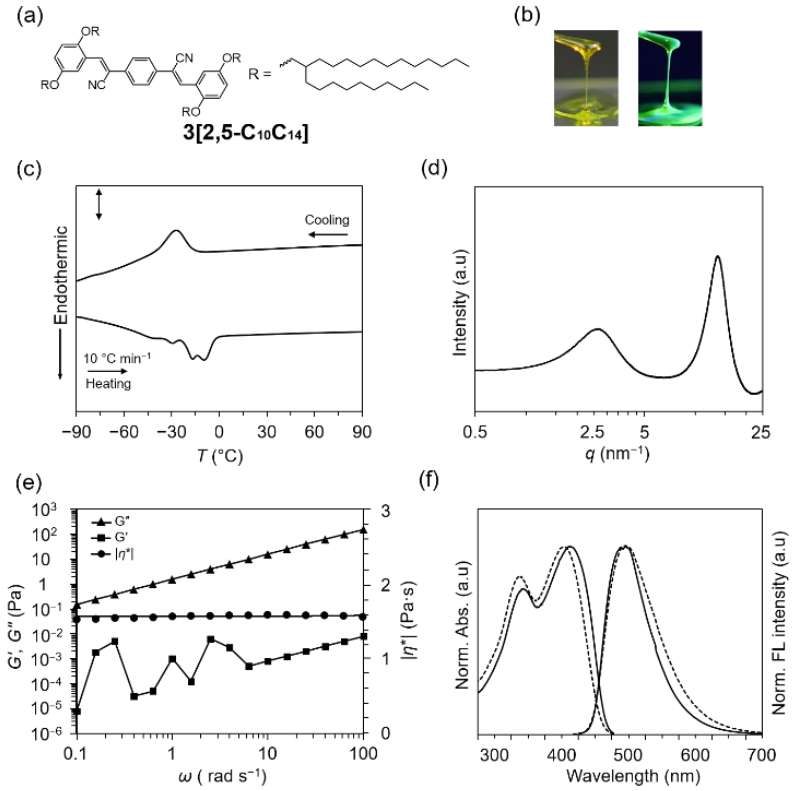

Figure 8. Properties of **3[2,5-C$_{10}$C$_{14}$]**: (a) Molecular structure. (b) Photo images under ambient light (left) and UV 365 nm irradiation (right) in the solvent-free liquid state at room temperature. (c) DSC thermogram from −90 to 90 °C at 10 °C min^{-1} (sb: 1 W g^{-1}). (d) SWAXS profile at 25 °C. (e) Storage elastic moduli (G', square), loss viscous moduli (G'', triangle), and complex viscosity (|η*|, circle) as a function of ω with γ = 0.1 at 25 °C in the solvent-free liquid state. (f) The normalized UV-Vis absorption and fluorescence spectra in the solvent-free liquid state (solid lines) and CH_2Cl_2 solution (dashed lines, UV-Vis: 10 μM; fluorescence: 0.2 μM) at room temperature.

The environment surrounding the chromophores often affects their optical features. For example, DCS analogues embedded in poly(methyl methacrylate) film exhibited red-shifted absorption compared to those in dilute solution,[28c] which was found in the case of **3[2,5-$C_{10}C_{14}$]**, too. The UV-Vis absorption spectra of **3[2,5-$C_{10}C_{14}$]** in the solvent-free liquid state exhibited a 10 nm red shift compared to that in the CH_2Cl_2 solution, while not showing broader characteristics (Figure 8f). The red shift might be explained by the concept of "twisted elasticity" whereby the intermolecular constraints between DCS molecules in the condensed liquid state could lead to partially increased planarization.[28e] The effect of the surrounding environment, such as the polarity, composed of the liquid itself, might also contribute. The onset and fluorescence λ_{max} in the solvent-free liquid state were close to those in the CH_2Cl_2 solution. Moreover, its CIE values exhibited similar luminescence colors. Therefore, the intrinsic absorption and fluorescence properties of **3[2,5-$C_{10}C_{14}$]** in CH_2Cl_2 solution are almost retained in the solvent-free liquid state. According to the above results, the 2,5-$C_{10}C_{14}$ substitution pattern for the DSB system is also applicable to constructing an alkyl–DCS liquid with similar liquid physical and optical superiorities, such as a comparable low viscosity.

Conclusion

The 2-decyltetradecyloxy chains at the (2,5-) substituent position of the terminal phenyl units were the substitution pattern for constructing a superior alkyl–distyrylbenzene (DSB) liquid, confirmed via modulation from the substituent position and alkyl chain length. The DSB liquid exhibited the lowest viscosity of 1.65 Pa·s as a thermodynamically stable liquid at room temperature, intrinsic optical properties from the DSB core unit as well as high thermal- and photo-stabilities. The correlation of 'structure–viscosity' in alkyl–DSB liquids thoroughly revealed that a smaller molecular size, faster molecular motion, and larger fractional free volume are advantageous for achieving a lower viscosity. In addition, the synergy between several optical characterizations, such as UV-Vis, fluorescence, and Raman spectroscopy as well as DFT calculations provided deeper insight into the effect of the substituent position on the optical properties in the solvent-free liquid state. Notably, the 2,5-$C_{10}C_{14}$ substitution pattern is also applicable to other π-conjugated molecules; an alkyl–dicyanostyrylbenzene liquid can be constructed with a similar superiority of liquid

physical and optical properties as seen in the alkyl–DSB liquid. Therefore, modulation of the substitution pattern is a useful molecular design and/or guiding strategy for constructing superior alkyl-π FMLs with rich optoelectronic properties. The current results will pave the way for the development of alkyl-π FMLs in deformable and flowable optoelectronic applications.

Author contributions

X.Z. performed the synthesis, characterization, theoretical calculation, and writing the original manuscript. K.N. commented on the outline of the manuscript and was involved in the discussion of the main results. T.T. performed the Raman experiments. K.H. performed the solid-state NMR experiments. T.N. conceived the main concept, and supervised, reviewed, and edited the manuscript. All authors discussed the results and commented on the manuscript.

Conflicts of interest

There are no conflicts to declare.

Acknowledgments

We acknowledge the financial support by the Grants-in-Aid for Scientific Research (JSPS KAKENHI Grant Number JP18H03922). The authors appreciate TOYOSEIKO CO., LTD. for measuring free volume by PSA. X.Z. thanks to the educational discussions with Dr. A. Shinohara, Dr. R. K. Gupta, and Dr. T. Machida at NIMS. X.Z. acknowledges the NIMS Jr. fellowship for the Hokkaido University-NIMS Joint Graduate School Program.

Data Availability Statement

The data that support this study are available in the supplementary material of this article.

Keywords: alkyl-π functional molecular liquids • distyrylbenzene • luminescence • substitution pattern modulation • viscosity

References

[1] a) C. Majidi, *Adv. Mater. Technol*. **2018**, *4*, 1800477; b) S. Grosjean, M. Wawryszyn, H. Mutlu, S. Bräse, J. Lahann and P. Theato, *Adv. Mater.* **2019**, *31*, 1806334; c) Z. Guo, H. Wang, J. Shao, Y. Shao, L. Jia, L. Li, X. Pu and Z. Wang, *Sci. Adv*. **2022**, *8*, eabo5201; d) S. Lee, Q. Shi and C. Lee, *APL Mater.* **2019**, *7*, 031302; e) Y. Wang, H. Haick, S. Guo, C. Wang, S. Lee, T. Yokota and T. Someya, *Chem. Soc. Rev.* **2022**, *51*, 3759–3793; f) Y. Jiang, Z. Zhang, Y.-X. Wang, D. Li, C.-T. Coen, E. Hwaun, G. Chen, H.-C. Wu, D. Zhong, S. Niu, W. Wang, A. Saberi, J.-C. Lai, Y. Wu, Y. Wang, A. A. Trotsyuk, K. Y. Loh, C.-C. Shih, W. Xu, K. Liang, K. Zhang, Y. Bai, G. Gurusankar, W. Hu, W. Jia, Z. Cheng, R. H. Dauskardt, G. C. Gurtner, J. B.-H. Tok, K. Deisseroth, I. Soltesz and Z. Bao, *Science* **2022**, *375*, 1411–1417.

[2] a) T. Nakanishi, *Functional organic liquids*, Wiley-VCH, Verlag GmbH & Co. KGaA **2019**; b) F. Lu and T. Nakanishi, *Sci. Technol. Adv. Mater.* **2015**, *16*, 014805.

[3] a) T. Michinobu, T. Nakanishi, J. P. Hill, M. Funahashi and K. Ariga, *J. Am. Chem. Soc.* **2006**, *128*, 10384–10385; b) T. Michinobu, K. Okoshi, Y. Murakami, K. Shigehara, K. Ariga and T. Nakanishi, *Langmuir* **2013**, *29*, 5337–5344; c) H. Li, S. S. Babu, S. T. Turner, D. Neher, M. J. Hollamby, T. Seki, S. Yagai, Y. Deguchi, H. Möhwald and T. Nakanishi, *J. Mater. Chem. C* **2013**, *1*, 1943–1951; d) M. J. Hollamby, M. Karny, P. H. H. Bomans, N. A. J. M. Sommerdjik, A. Saeki, S. Seki, H. Minamikawa, I. Grillo, B. R. Pauw, P. Brown, J. Eastoe, H. Möhwald and T. Nakanishi, *Nat. Chem.* **2014**, *6*, 690–696.

[4] a) S. S. Babu, J. Aimi, H. Ozawa, N. Shirahata, A. Saeki, S. Seki, A. Ajayaghosh, H. Möhwald and T. Nakanishi, *Angew. Chem. Int. Ed.* **2012**, *51*, 3391–3395; b) S. S. Babu, M. J. Hollamby, J. Aimi, H. Ozawa, A. Saeki, S. Seki, K. Kobayashi, K. Hagiwara, M. Yoshizawa, H. Möhwald and T. Nakanishi, *Nat. Commun.* **2013***, 4,* 1969*;* c) F. Lu, T. Takaya, K. Iwata, I. Kawamura, A. Saeki, M. Ishii, K. Nagura and T. Nakanishi, *Sci. Rep.* **2017**, *7*, 3416; d) B. Narayan, K. Nagura, T. Takaya, K. Iwata, A. Shinohara, H. Shinmori, H. Wang, Q. Li, X. Sun, H. Li, S. Ishihara and T. Nakanishi, *Phys. Chem. Chem. Phys.* **2018**, *20*, 2970–2975; e) F. Lu, K. Hagiwara, M. Yoshizawa, K. Nagura, S. Ishihara and T. Nakanishi, *J. Mater. Chem. C* **2019**, *7*, 2577–2582; f) F. Lu and T. Nakanishi, *Adv. Opt. Mater.* **2019**, *7*, 1900176; g) Goudappagouda, A. Manthanath, V. C. Wakchaure, K. C. Ranjeesh, T. Das, K. Vanka, T. Nakanishi and S. S. Babu, *Angew. Chem. Int. Ed.* **2019**, *58*, 2284–2288.

[5] a) A. Ghosh, M. Yoshida, K. Suemori, H. Isago, N. Kobayashi, Y. Mizutani, Y. Kurashige, I. Kawamura, M. Nirei, O. Yamamuro, T. Takaya, K. Iwata, A. Saeki, K. Nagura, S. Ishihara and T. Nakanishi, *Nat. Commun.* **2019**, *10*, 4210; b) T. Ogoshi, K. Maruyama, Y. Sakatsume, T. Kakuta, T. Yamagishi, T. Ichikawa and M. Mizuno, *J. Am. Chem. Soc.* **2019**, *141*, 785–789; c) A. Zielinska, A. Takai, H. Sakurai, A. Saeki, M. Leonowicz and T. Nakanishi, *Chem. Asian J.* **2018**, *13*, 770–774; d) Y. Chino, T. Nakanishi and M. Kimura, *New J. Chem.* **2020**, *44*, 1689–1693.

[6] a) A. Shinohara, C. Pan, Z. Guo, L. Zhou, Z. Liu, L. Du, Z. Yan, F. J. Stadler, L. Wang and T. Nakanishi, *Angew. Chem. Int. Ed.* **2019**, *58*, 9581–9585; b) Z. Guo, A. Shinohara, C. Pan, F. J. Stadler, Z. Liu, Z.-C. Yan, J. Zhao, L. Wang and T. Nakanishi, *Mater. Horiz.* **2020**, *7*, 1421–1426; c) A. Shinohara, M. Yoshida, C. Pan, and T. Nakanishi, *Polym. J.* **2022**, https://doi.org/10.1038/s41428-022-00725-w.

[7] a) D. Xu and C. Adachi, *Appl. Phys. Lett.* **2009**, *95*, 053304; b) N. Kobayashi, T. Kasahara, T. Edura, J. Oshima, R. Ishimatsu, M. Tsuwaki, T. Imato, S. Shoji and J. Mizuno, *Sci. Rep.* **2015**, *5*, 14822; c) M. Kawamura, H. Kuwae, T. Kamibayashi, J. Oshima, T. Kasahara, S. Shoji and J. Mizuno, *Sci. Rep.* **2020**, *10*, 14528.

[8] a) M. Gervaldo, M. Funes, J. Durantini, L. Fernandez, F. Fungo and L. Otero, *Electrochim.* **2010**, *55*, 1948–1957; b) P. Z. Crocomo, M. Okazaki, T. Hosono, S. Minakata, Y. Takeda and P. Data, *Chem. Eur. J.* **2022**, e202200826.

[9] Q. Huang, G. Zhuang, H. Jia, M. Qian, S. Cui, S. Yang and P. Du, *Angew. Chem. Int. Ed.* **2019**, *58*, 6244–6249.

[10] a) C. Allain, J. Piard, A. Brosseau, M. Han, J. Paquier, T. Marchandier, M. Lequeux, C. Boissière and P. Audebert, *ACS Appl. Mater. Interfaces* **2016**, *8*, 19843–19846; b) M. P. Dominguez, B. Demirkurt, M. Grzelka, D. Bonn, L. Galmiche, P. Audebert and A. M. Brouwer, *Molecules* **2021**, *26*, 6047.

[11] a) K. Chung, M. S. Kwon, B. M. Leung, A. G. Wong-Foy, M. S. Kim, J. Kim, S. Takayama, J. Gierschner, A. J. Matzger and J. Kim, *ACS Cent. Sci.* **2015**, *1*, 94–102; b) T. Machida, R. Taniguchi, T. Oura, K. Sada and K. Kokado, *Chem. Commun.* **2017**, *53*, 2378–2381; c) F. Lu, K. Jang, I. Osica, K. Hagiwara, M. Yoshizawa, M. Ishii, Y. Chino, K. Ohta, K. Ludwichowska, K. J. Kurzydłowski, S. Ishihara and T. Nakanishi, *Chem. Sci*. **2018**, *9*, 6774-6778; d) Y. Sato, Y. Mutoh, S. Morishita, N. Tsurumachi and K. Isoda, *J. Phys. Chem. Lett.* **2021**, *12*, 3014–3018.

[12] a) T. Ikuta, W. Shihoya, M. Sugiura, K. Yoshida, M. Watari, T. Tokano, K. Yamashita, K. Katayama, S. P. Tsunoda, T. Uchihashi, H. Kandori and O. Nureki, *Nat. Commun.* **2020**, *11*, 5605; b) J. G. Monroe, T. Srikant, P. Carbonell-Bejerano, C. Becker, M. Lensink, M. Exposito-Alonso, M. Klein, J. Hildebrandt, M. Neumann, D. Kliebenstein, M.-L. Weng, E. Imbert, J. Ågren, M. T. Rutter, C. B. Fenster and D. Weigel, *Nature* **2022**, *602*, 101–105.

[13] a) Z. Zhang, C.-L. Chen, Y.-A. Chen, Y.-C. Wei, J. Su, H. Tian and P.-T. Chou, *Angew. Chem. Int. Ed.* **2018**, *57*, 9880–9884; b) A. Wicklein, A. Lang, M. Muth and M. Thelakkat, *J. Am. Chem. Soc.* **2009**, *131*, 14442–14453; c) T. A. Turkmen, L. Zeng, Y. Cui, İ. Fidan, F. Dumoulin, C. Hirel, Y. Zorlu, V. Ahsen, A. A. Chernonosov, Y. Chumakov, K. M. Kadish, A. G. Gürek and S. T. Öztürk, *Inorg. Chem.* **2018**, *57*, 6456–6465; d) J. Kumagai, K. Hirano, T. Satoh, S. Seki and M. Miura, *J. Phys. Chem. B* **2011**, *115*, 8446–8452.

[14] a) A. Heller, *J. Chem. Phys.* **1964**, *40*, 2839–2851; b) T. E. Bush and G. W. Scott, *J. Phys. Chem.* **1981**, *85*, 144–146; c) R. C. Smith, L. B. Gleason and J. D. Protasiewicz, *J. Mater. Chem.* **2006**, *16*, 2445–2452; d) S. Varghese, S. K. Park, S. Casado, R. C. Fischer, R. Resel, B. Milián-Medina, R. Wannemacher, S. Y. Park and J. Gierschner, *J. Phys. Chem. Lett.* **2013**, *4*, 1597–1602; e) J. Gierschner, L. Lüer, B. Milián-Medina, D. Oelkrug and H.-J. Egelhaaf, *J. Phys. Chem. Lett.* **2013**, *4*, 2686–2697; f) J. Gierschner and S. Y. Park, *J. Mater. Chem. C* **2013**, *1*, 5818–5832.

[15] a) M. M. Rueda, M.-C. Auscher, R. Fulchirona, T. Périé, G. Martin, P. Sonntag, P. Cassagnaua, *Prog. Polym. Sci.* **2017**, *66*, 22–53. b) H. Münstedt, and F. R. Schwarzl, *Rheological Properties and Molecular Structure*, *Deforemation and Flow of Polymeric Material*, Springer, **2014**, Ch. 13, 420–452.

[16] a) G. Yu, D. Zhao, L. Wen, S. Yang, and X. Chen, *AIChE J*. **2012**, *58*, 2885–2899; b) R. Alcalde, G. García, M. Atilhan and S. Aparicio, *Ind. Eng. Chem. Res.* **2015**, *54*, 10918–10924.

[17] a) R. H. Ewell and H. Eyring, *J. Chem. Phys.* **1937**, *5*, 726–736; b) R. Simha, *J. Chem. Phys.* **1939**, *7*, 202–203; c) H. Eyring and T. Ree, *Proc. Natl. Acad. Sci.* **1961**, *47*, 526–537; d) A. Allal, C. Boned, and A. Baylaucq, *Phys. Rev. E,* **2001**, *64*, 011203; e) A. Bondi, *Viscosity and Molecular Structure*, *Rheology*, Vol. 4, Elsevier, **1967**, Ch. 1.

[18] a) M. H. Cohen and D. Turnbull, *J. Chem. Phys.* **1959**, *31*, 1164–1169; b) A. K. Doolittle, *J. Appl. Phys.*, **1951**, *22*, 1471–1475; c) A. A. Miller, *J. Phys. Chem.* **1963**, *67*, 1031–1035; d) D. B. Davies and A. J. Matheson, *J. Chem. Phys.* **1966**, *45*, 1000–1006; e) H. Rötger, *J. Non. Cryst. Solids* **1974**, *14*, 201–217; f) I. Bandrés, B. Giner, I. Gascón, M. Castro and C. Lafuente, *J. Phys. Chem. B* **2008**, *112*, 12461–12467; g) K. R. Harris, *J. Chem. Phys.* **2009**, *131*, 054503; h) A. A. Miller, *J. Chem. Phys.* **1963**, *38*, 1568–1571; i) R. H. Ewell and H. Eyring, *J. Chem. Phys.* **1937**, *5*, 726–736.

[19] a) D. D. Laws, Bitter, H. M. L. Bitter and A. Jerschow, *Angew. Chem. Int. Ed.* **2002**, *41*, 3096–3129; b) H. Saitô, I. Ando and A. Naito, *Solid state NMR spectroscopy for Biopolymers: Principles and Applications,* Springer, Netherlands, **2006**.

[20] a) S. J. Tao, *J. Chem. Phys.* **1972**, *56*, 5499–5510; b) M. Eldrup, *Chem. Phys*. **1981**, *63*, 51–58; c) T. Goworek, *J. Nucl. Radiochem. Sci.* **2000**, *1*, 11–13; d) K. Tanaka, K.-I. Okamoto, H. Kita and Y. Ito, *Polym. J.* **1993**, *25*, 577–584; e) V. P. Shantarovich, I. B. Kevdina, Y. P. Yampolskii and A. Y. Alentiev, *Macromolecules* **2000**, *33*, 7453–7466; f) X. Hong, Y. C. Jean, H. Yang, S. S. Jordan and W. J. Koros, *Macromolecules* **1996**, *29*, 7859–7864.

[21] D. Rauber, F. Philippi, B. Kuttich, J. Becker, T. Kraus, P. Hunt, T. Welton, R. Hempelmann and C. W. M. Kay, *Phys. Chem. Chem. Phys.* **2021**, *23*, 21042–21064.

[22] a) M. Zatloukai, *Polymer* **2016**, *104*, 258–267; b) J.-D. Jeon, S.-Y. Kwak, and B.-W. Cho, *J. Electrochem*. **2005**, *152*, 1583–1589; c) P. Xiang, R. Zhang, M. Niu, X. Guo, and Q. Bai, *Adv. Mat. Res.* **2011**, *332–334*, 949–954; d) S. Fang, L. Yang, C. Wei, C. Peng, K. Tachibana and K. Kamijima, *Electrochem. Commun*. **2007**, *9*, 2696–2702; e) O. O. Okoturo, T. J. Vandernoot, *J. Electroanal. Chem*. **2004**, *568*, 167–181.

[23] a) S.-H. Lim, T. G. Bjorklund and C. J. Bardeen, *J. Phys. Chem. B* **2004**, *108*, 4289–4295; b) A. Masunov, S. Tretiak, *J. Chem. Phys.* **2005**, *122*, 224505; c) H.-J. Egelhaaf, J. Gierschner and D. Oelkrug, *Synth. Met.* **2002**, *127*, 221–227.

[24] J. C. Walsh, D. T. Hogan, K.-L. M. Williams, S. D. Brake, G. Venkataramana, T. A. Misener, B. J. Wallace, R. P. Johnson, D. W. Thompson, Y. Zhao, B. D. Wagner, and G. J. Bodwell, *ChemPlusChem* **2019**, *84*, 754–765.

[25] a) H. G. Kim, M. Kim, J. A. Clement, J. Lee, J. Shin, H. Hwang, D. H. Sin and K. Cho, *Chem. Mater.* **2015**, *27*, 6858–6868; b) B. Pal, W.-C. Yen, J.-S. Yang, and W.-

F. Su, *Macromolecules* **2007**, *40*, 8189–8194; c) L. Huo, S. Zhang, X. Guo, F. Xu, Y. Li and J. Hou, *Angew. Chem. Int. Ed.* **2011**, *50*, 9697–9702.

[26] a) L. Ma, X. Wang, B. Wang, J. Chen, J. Wang, K. Huang, B. Zhang, Y. Cao, Z. Han, S. Qian and S. Yao, *Chem. Phys.* **2002**, *285*, 85–94; b) E. Stadler, A. Eibel, D. Fast, H. Freißmuth, C. Holly, M. Wiech, N. Moszner and G. Gescheidt, *Photochem. Photobiol. Sci.* **2018**, *17*, 660–669.

[27] a) B. Tian and G. Zerbi, *J. Chem. Phys.* **1991**, *95*, 3191–3197; b) A. Sakamoto, Y. Furukawa and M. Tasumi, *J. Phys. Chem.* **1992**, *96*, 1490–1494; c) T. Hrenar, R. Mitrić, Z. Meić, H. Meier and U. Stalmach, *J. Mol. Struct.* **2003**, *661–662*, 33–40; d) M. Edelson and A. Bree, *Chem. Phys. Lett.* **1976**, *41*, 562–564; e) A. Bree and M. Edelson, *Chem. Phys.* **1980**, *51*, 77–88; f) K. Honda, Y. Furukawa and H. Nishide, *Vib. Spectrosc.* **2006**, *40*, 149–154; g) B. M. Auer and J. L. Skinner, *J. Chem. Phys.* **2008**, *128*, 224511.

[28] a) T. Lei, J.-Y. Wang and J. Pei, *Chem. Mater.* **2014**, *26*, 594–603; b) Y. Haketa, Y. Bando, Y. Sasano, H. Tanaka, N. Yasuda, I. Hisaki, H. Maeda, iScience, **2019**, *14*, 241–256; c) K. Nakamura, S. Sugiura, F. Araoka, S. Aya, Y. Takanishi, G. Watanabe, R. Sato, Y. Shigeta, and H. Maeda, *Org. Lett*. **2021**, *23*, 305–310; d) F. Lu, E. A. Neal and T. Nakanishi, *Acc. Chem. Res.* **2019**, *52*, 1834–1843; e) E. A. Neal and T. Nakanishi, *Bull. Chem. Soc. Jpn*. **2021**, *94*, 1769–1788.

[29] a) C. Löwe and C. Weder, *Adv. Mater.* **2002**, *14*, 1625–1629; b) J. Kunzelman, M. Kinami, B. R. Crenshaw, J. D. Protasiewicz and C. Weder, *Adv. Mater.* **2008**, *20*, 119–122; c) J. Shi, L. E. A. Suarez, S.-J. Yoon, S. Varghese, C. Serpa, S. Y. Park, L. Lüer, D. Roca-Sanjuán, B. Milián-Medina and J. Gierschner, *J. Phys. Chem. C* **2017**, *121*, 23166–23183; d) S.-J. Yoon, J. H. Kim, K. S. Kim, J. W. Chung, B. Heinrich, F. Mathevet, P. Kim, B. Donnio, A.-J. Attias, D. Kim and S. Y. Park, *Adv. Funct. Mater.* **2012**, *22*, 61–69; e) J. Shi, S.-J. Yoon, L. Viani, S. Y. Park, B. Milián-Medina and J. Gierschner, *Adv. Opt. Mater.* **2017**, *5*, 1700340.